J|A|C|S
ARTICLES
Published on Web 10/06/2004

Structural Characterization of Modular Supramolecular Architectures in Solution

David M. Tiede*,[†] Ruitian Zhang,[†] Lin X. Chen,[†] Lianhe Yu,[‡] and Jonathan S. Lindsey[‡]

Contribution from the Chemistry Division, Argonne National Laboratory, Argonne, Illinois 60439 and the Department of Chemistry, North Carolina State University, Raleigh, North Carolina 27695

Received March 29, 2004; E-mail: tiede@anl.gov

Abstract: Structures of modular supramolecular architectures consisting of a hexameric, diphenylethyne-linked porphyrin macrocyclic array and the corresponding host−guest complex formed by inclusion of a tripyridyl guest molecule were characterized in solution using high-angle X-ray scattering. Scattering measurements made to 6 Å resolution coupled with pair distance function (PDF) analyses demonstrated that (1) the porphyrin architectures are not rigid but are distributed across a conformational ensemble with a mean diameter that is 1.5 Å shorter than the diameter of a symmetric, energy-minimized model structure, (2) the conformational envelope has limits of 3 Å positional dispersion and full rotational freedom for all six porphyrin groups, and (3) insertion of the tripyridyl guest molecule expands the diameter of the host conformer by 0.6 Å and decreases the configurational dispersion by approximately 2-fold. These results validate the molecular design, provide a new measure of conformational ensembles in solution that cannot be obtained by other techniques, and establish a structural basis for understanding the photophysical and guest−hosting functions of the hexameric porphyrin architectures in liquids.

Introduction

The syntheses of supramolecular architectures with nanometer-scale, shape-persistent conformations based on covalent connectivity represent remarkable achievements with impact across a broad range of biomimetic and materials chemistry.[1−3] Synthetic capabilities have advanced to the point where supramolecular architectures and conformational flexibilities can be tuned to achieve selected host−guest,[4−6] dynamic,[7] and adaptive[8−10] properties. To confer structural definition, many architectures are composed of somewhat rigid building blocks in macrocyclic or macropolycyclic geometries. Indeed, members of a new class of macrocyclic architectures are referred to as "shape-persistent" in recognition of the expected ability of the molecules to retain their structure-dictated shape in diverse media. However, experimental validations of synthetic designs for supramolecular architectures and subsequent correlation to chemical function are significantly hindered by the lack of methods for resolving structure and dynamics of supramolecular architectures in liquids and other functionally relevant noncrystalline media.

Challenges for structural characterization are particularly severe for modular supramolecular architectures possessing conformational complexity, adaptive structures, and building block compositions. For example, structural complexity and conformational flexibility have limited the success of crystallographic approaches for characterization of large supramolecular architectures.[1−3,11] Even with successful crystallographic structure determination, questions remain concerning the conformational landscapes occupied by the supramolecular architectures in noncrystalline liquid states. Repetitive building blocks with chemically analogous groups restrict the use of multidimensional NMR techniques for resolving spatial relationships within the supramolecular architectures.[1,2,11] Spectroscopy and mass spectrometry have typically provided critical evidence for proof of composition and allow deduction of general features of supramolecular architectures, but these techniques do not provide direct measures of conformational structures. Static (SLS) and dynamic (DLS) light scattering can be used to measure the effective size of a particle (radius of gyration and hydration, respectively), and indirectly to infer its shape, but the wavelengths of visible and UV light prevent direct resolution of internal structure for supramolecular architectures with dimensions smaller than ∼100 nm.[12,13] For supramolecular

[†] Argonne National Laboratory.
[‡] North Carolina State University.

(1) Moore, J. S. *Acc. Chem. Res.* **1997**, *30*, 402−413.
(2) Grave, C.; Schlüter, A. D. *Eur. J. Org. Chem.* **2002**, 3075−3098.
(3) Höger, S. *J. Polym. Sci., Part A: Polym. Chem.* **1999**, *37*, 2685−2698.
(4) Yu, L.; Lindsey, J. S. *J. Org. Chem.* **2001**, *66*, 7402−7419.
(5) Tomizaki, K.-Y.; Yu, L.; Wei, L.; Bocian, D. F.; Lindsey, J. S. *J. Org. Chem.* **2003**, *68*, 8199−8207.
(6) Höger, S.; Meckenstock, A.-D. *Chem. Eur. J.* **1999**, *5*, 1686−1691.
(7) Furlan, R. L. E.; Otto, S.; Sanders, J. K. M. *Proc. Natl. Acad. Sci. U.S.A.* **2002**, *99*, 4801−4804.
(8) Chong, Y. S.; Shimizu, K. D. *Synthesis* **2002**, *9*, 1239−1244.
(9) Höger, S.; Morrison, D. L.; Enkelmann, V. *J. Am. Chem. Soc.* **2002**, *124*, 6734−6736.
(10) Gianneschi, N. C.; Bertin, P. A.; Nguyen, S. T.; Mirkin, C. A.; Zakharov, L. N.; Rheingold, A. L. *J. Am. Chem. Soc.* **2003**, *125*, 10508−10509.
(11) Grave, C.; Lentz, D.; Schäfer, A.; Samori, P.; Rabe, J. P.; Franke, P.; Schlüter, A. D. *J. Am. Chem. Soc.* **2003**, *125*, 6907−6918.
(12) Cotton, J. P. In *Neutron, X-ray and Light Scattering*; Lindner, P., Zemb, T., Eds.; Elsevier Science Publishers B. V.: Amsterdam, 1991; pp 3−18.
(13) Glatter, O. In *Neutron, X-ray and Light Scattering;* Lindner, P., Zemb, T., Eds.; Elsevier Science Publishers B. V.: Amsterdam, 1991; pp 33−82.

10.1021/ja048209q CCC: $27.50

architectures that self-assemble via noncovalent bonds, measurements of colligative properties (e.g., vapor-phase osmometry),[14−16] sedimentary behavior (e.g., density centrifugation),[17,18] or chromatographic behavior (e.g., size-exclusion chromatography)[19] have often been employed to establish the size of the assemblies. In general, there remains a pressing need for methods of structural determination that can be applied to supramolecular architectures in diverse types of condensed media.

The availability of high-flux, third-generation synchrotron X-ray sources and the development of large area solid-state detectors have opened up new opportunities for structural analysis of macromolecules in liquids through measurement of wide-angle X-ray scattering.[20−23] Scattering patterns are the rotationally averaged interference produced by collective intramolecular atomic scattering and are related to the atomic pair distance distribution function (PDF) by Fourier transform.[24,25] The ability to deduce structure from scattering and PDF data is determined to a large extent by the complexity of the molecular system. For large macromolecular assemblies such as proteins and micelles, wide-angle scattering features are diffuse and contain overlapping contributions from many structural elements.[20−23,26,27] For small molecules, PDF patterns show well-resolved, discrete features that can yield a complete resolution of molecular structure and dynamics at the atomic scale, as has been elegantly demonstrated for small hydrocarbon and halogenated hydrocarbon molecules in the gas phase using electron-scattering techniques.[28−32] Clear opportunities exist for structural characterization of "shape-persistent" macrocycles in solution using analogous high-angle X-ray scattering because such macrocycles often have structural complexity that is intermediate between those of proteins and small molecules. However, special challenges lie first in the demonstration that high-resolution X-ray scattering data can be acquired for aromatic macrocycles in organic solvents of nearly equivalent electron density and second in the development of analytical tools for interpreting scattering and PDF data in terms of structurally relevant parameters.

We have investigated opportunities for structural characterization of modular supramolecular architectures in solution using wide-angle scattering by performing initial characterization studies on a diphenylethyne-linked porphyrin architecture **1** comprised of a cyclic array of alternating Zn and free-base porphyrin groups and its corresponding host−guest complex, **1**+**2**, formed by complexation of **1** with the tripyridyl guest molecule **2**,[4,5,33−35] illustrated in Scheme 1. The binding affinity of **1**+**2** is sufficiently strong ($K_{assoc} > 3 \times 10^8$ M^{-1}) that the complex is largely associated at micromolar concentrations. A wide variety of multiporphyrin arrays have been prepared for studies related to biological and materials chemistry.[35−41] The hexameric porphyrin architecture **1** is of particular interest because of the design for photochemistry and energy transfer,[33,34] the capacity for being customized to host a variety of photochemically active guest molecules,[4,34] and the potential for serving as a building block for columnar assemblies.[5] Compound **1** and its related host−guest complexes have resisted structural characterization by crystallographic and NMR techniques. The designs of molecular guests are based on models that have estimated the macrocycle diameter to be approximately 35 Å. The hexameric wheel structure and the hosting capabilities have been validated by spectroscopic, photochemical, and mass spectral techniques without resolving specific structural characteristics.[4,5,33−35]

In this paper, we demonstrate the ability to accurately characterize the shapes of macrocycle **1** and host−guest assembly **(1**+**2)** in aromatic hydrocarbon solvents using high-angle X-ray scattering techniques. Experimental scattering patterns measured to 6 Å resolution are shown to resolve individual porphyrin pair distance correlations and to identify molecular thermal factors or configuration dispersion through measurement of the angle-dependent attenuation of the wide-angle scattering features. In addition, analytical tools are introduced for interpreting configurational dispersion in terms of energy-minimized structures and rigid-body motions of composite porphyrin building blocks. This work establishes the general applicability of high-angle scattering data for structural characterization of shape-persistent supramolecular architectures in liquids.

Results and Discussion

Model Structures. Model structures for the cyclic Zn_3Fb_3 porphyrin hexamer **1** and the complex formed between the cyclic Zn_3Fb_3 porphyrin hexamer and the tripyridyl guest **1**+**2** were generated by model building and energy minimization using

(14) Seto, C. T.; Whitesides, G. M. *J. Am. Chem. Soc.* **1993**, *115*, 905−916.
(15) Nelson, J. C.; Saven, J. G.; Moore, J. S.; Wolynes, P. G. *Science* **1997**, *277*, 1793−1796.
(16) Higler, I.; Grave, L.; Breuning, E.; Verboom, W.; De Jong, F.; Fyles, T. M.; Reinhoudt, D. N. *Eur. J. Org. Chem.* **2000**, 1727−1734.
(17) Langerman, N. R.; Klotz, I. M. *Biochemistry* **1969**, *8*, 4746−4752.
(18) Schubert, D.; Tziatzios, C.; Schuck, P.; Schubert, U. S. *Chem. Eur. J.* **1999**, *5*, 1377−1383.
(19) Corbin, P. S.; Lawless, L. J.; Li, Z. M. Y.; Witmer, M. J.; Zimmerman, S. C. *Proc. Natl. Acad. Sci. U.S.A.* **2002**, *99*, 5099−5104.
(20) Zhang, R.; Thiyagarajan, P.; Tiede, D. M. *J. Appl. Crystallogr.* **2000**, *33*, 565−568.
(21) Tiede, D. M.; Zhang, R.; Seifert, S. *Biochemistry* **2002**, *41*, 6605−6614.
(22) Hirai, M.; Iwase, H.; Hayakawa, T.; Miura, K.; Inoue, K. *J. Synchrotron Rad.* **2002**, *9*, 202−205.
(23) Fischetti, R. F.; Rodi, D. J.; Mirza, A.; Irving, T. C.; Kondrashkina, E.; Makowski, L. *J. Synchrotron Rad.* **2003**, *10*, 398−404.
(24) Svergun, D.; Barberato, C.; Koch, M. H. J. *J. Appl. Crystallogr.* **1995**, *28*, 768−773.
(25) Svergun, D. I. *J. Appl. Crystallogr.* **1992**, *25*, 495−503.
(26) Petoukhov, M. V.; Eady, N. A. J.; Brown, K. A.; Svergun, D. I. *Biophys. J.* **2002**, *83*, 3113−3125.
(27) Svergun, D. I.; Petoukhov, M. V.; Koch, M. H. J. *Biophys. J.* **2001**, *80*, 2946−2953.
(28) Williamson, J. C.; Cao, J.; Ihee, H.; Frey, H.; Zewail, A. H. *Nature* **1997**, *386*, 159−162.
(29) Ihee, H.; Goodson, B. M.; Srinivasan, R.; Lobastov, V. A.; Zewail, A. H. *J. Phys. Chem. A* **2002**, *106*, 4087−4103.
(30) Ihee, H.; Lobastov, V. A.; Gomez, U. M.; Goodson, B. M.; Srinivasan, R.; Ruan, C.-Y.; Zewail, A. H. *Science* **2001**, *291*, 458−462.
(31) Cao, J.; Ihee, H.; Zewail, A. H. *Proc. Natl. Acad. Sci. U.S.A.* **1999**, *96*, 338−342.
(32) Dudek, R. C.; Weber, P. M. *J. Phys. Chem. A* **2001**, *105*, 4167.
(33) Li, J.; Ambroise, A.; Yang, S. I.; Diers, J. R.; Seth, J.; Wack, C. R.; Bocian, D. F.; Holten, D.; Lindsey, J. S. *J. Am. Chem. Soc.* **1999**, *121*, 8927−8940.
(34) Ambroise, A.; Li, J.; Yu, L.; Lindsey, J. S. *Org. Lett.* **2000**, *2*, 2563−2566.
(35) Holten, D.; Bocian, D. F.; Lindsey, J. S. *Acc. Chem. Res.* **2002**, *35*, 57−69.
(36) Harvey, P. D. In *The Porphyrin Handbook*; Kadish, K. M., Smith, K. M., Guilard, R., Eds.; Academic Press: San Diego, CA, 2003; Vol. 18, pp 63−250.
(37) Burrell, A. K.; Officer, D. L.; Plieger, P. G.; Reid, D. C. W. *Chem. Rev.* **2001**, *101*, 2751−2796.
(38) Chambron, J.-C.; Heitz, V.; Sauvage, J.-P. In *The Porphyrin Handbook*; Kadish, K. M., Smith, K. M., Guilard, R., Eds.; Academic Press: San Diego, CA, 2000; Vol. 6, pp 1−42.
(39) Imamura, T.; Fukushima, K. *Coord. Chem. Rev.* **2000**, *198*, 133−136.
(40) Wojaczynski, J.; Latos-Grazynski, L. *Coord. Chem. Rev.* **2000**, *204*, 113−171.
(41) Chou, J.-H.; Kosal, M. E.; Nalwa, H. S.; Rakow, N. A.; Suslick, K. S. In *The Porphyrin Handbook*; Kadish, K. M., Smith, K. M., Guilard, R., Eds.; Academic Press: San Diego, CA, 2003; Vol. 3, pp 347−368.

Scheme 1

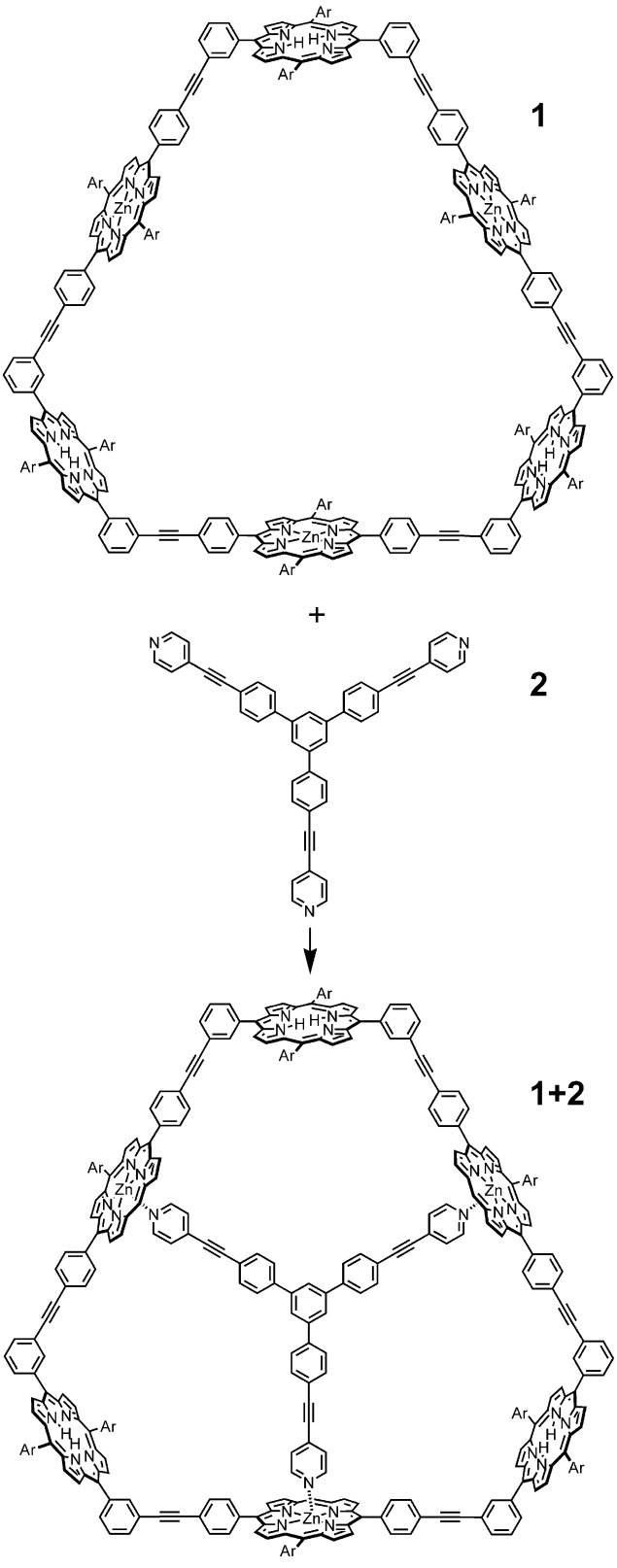

HyperChem (Hypercube). Details of the modeling are discussed in the Supporting Information. The inherent flexibility of the diphenylethyne and porphyrin groups creates a complex landscape of widely differing structures of comparable configurational energy that is potentially accessible for the hexameric porphyrin macrocycle in solution. This configurational flexibility

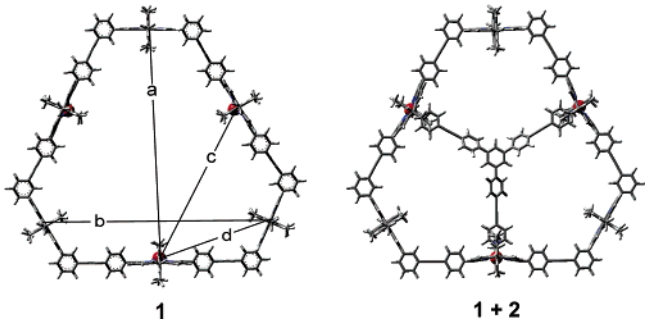

Figure 1. Energy-minimized conformers for architectures **1** and **1**+**2** produced by minimization starting from a threefold symmetric structure for assembly **1** having each of the porphyrin and aryl rings in perpendicular orientations. The conformer **1**+**2** was produced by inserting the guest **2** into the minimized conformer **1** and re-minimizing. Zinc atoms are rendered in CPK atomic volume representations.

was reflected in energy-minimization studies by a tendency for the hexameric porphyrin macrocycle to converge on conformers that represent local minima determined by the initial starting structures. In particular, modeling studies showed a strong interplay between the relative orientations of the aryl and porphyrin rings on doming and ruffling distortions of the porphyrin groups with corresponding distortions in torsions and in dihedral angles of the diphenylethyne linkers.

Energy-minimized conformers for architectures **1** and **1**+**2** shown in Figure 1 were obtained from a starting structure for architecture **1** wherein each of the aryl and attached porphyrin rings were positioned in perpendicular orientations with respect to each other. The perpendicular orientations of the aryl−porphyrin groups were not changed during the minimization, but slight distortions to the angles between the "corner-forming" *m*-aryl substituents and bowing distortions of the Zn−porphyrin groups and attached diphenylethyne linkers introduced slight asymmetry to the macrocyle geometry. Specific conformers can be characterized by center-to-center separations of the four discrete sets of porphyrin pairs in the cyclic architectures marked in Figure 1. For the minimized structure **1**, the averaged porphyrin pair separations were 33.8 Å (a), 32.7 Å (b), 25.8 Å (c), and 17.3 Å (d). Insertion of the tripyridyl guest **2** into the minimized structure **1**, followed by reminimization, resulted in the structure **1**+**2** shown in Figure 1. The configuration energy of **1**+**2** was lowered by about 25% compared to that of **1**, and the only significant change in structure was a slight inward bowing of the Zn−porphyrin groups that resulted in a 1.5 Å shortening of the center-to-center distances for the pairs a. The energetic stabilization and absence of significant distortion following guest insertion validates the molecular design strategy.

Several alternate conformers could be generated for architecture **1** by energy minimization starting with aryl−porphyrin planes positioned in nonperpendicular orientations. Such conformers showed significant doming and ruffling of the porphyrin groups that were coupled to torsional and dihedral distortions of the diphenylethyne linkers. The distortions were reflected in significant reduction in the threefold symmetry of the cyclic model architecture, including conformers that showed greater than 4 Å shifts in individual porphyrin pair distances found in structure **1**. An experimental challenge lies in determining whether such conformers are realistic representations of the molecular structures in solution.

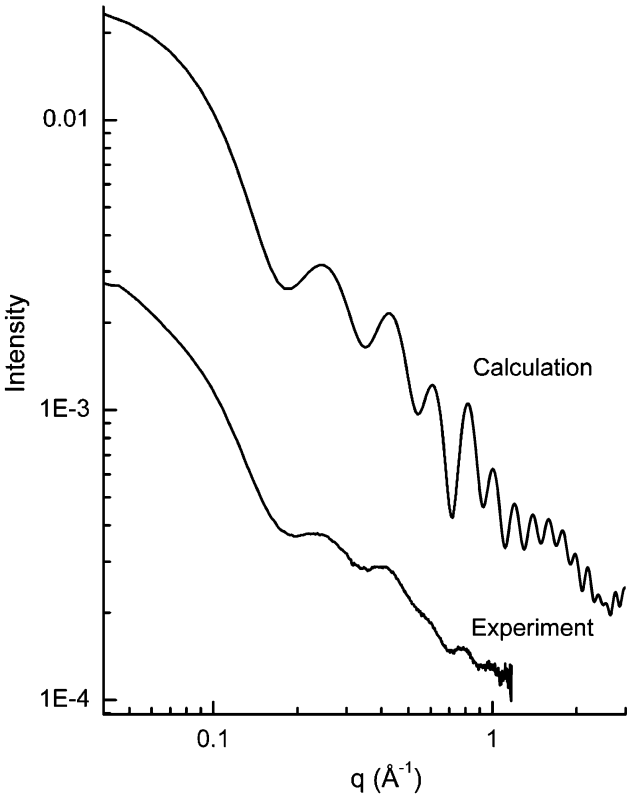

Figure 2. Calculated and experimental scattering data for architecture **1**. The upper trace shows the scattering pattern calculated using the coordinates of the energy-minimized conformer **1**. The lower trace is the experimental scattering pattern measured for a 1 mM solution of macrocycle **1** in toluene. The scattering pattern was recorded with 100 seconds of data acquisition time and a sample flow a rate of 50×10^{-6} l/min.

General Features of X-ray Scattering for Porphyrin Assemblies. The X-ray scattering pattern calculated for the energy-minimized model structure **1** in toluene is shown in the upper trace in Figure 2. The scattered pattern is plotted with arbitrary vertical scaling as a function of the magnitude of the scattering vector, **q**, which is related to the scattering angle 2θ by the relation $q = (4\pi/\lambda)\sin\theta$, where λ is the X-ray wavelength. The scattering pattern for the model structure was calculated to a resolution defined by $q = 3$ Å^{-1}, which corresponds to a spatial resolution, $d = 2\pi/q$, of 2.1 Å. In the low-resolution scattering region below $q = 0.1$ Å^{-1}, the electron-density variation across the molecular array cannot be resolved and the calculated scattering follows the Guinier relationship, $I(q) = I(0)\exp(-q^2R_g^2/3)$, parametrized in terms of the forward scattering amplitude, $I(0)$, and the radius of gyration, R_g.[42] The scattering amplitude, $I(0)$, is proportional to the electron-density contrast-weighted square of the number of electrons in the molecule. The parameter R_g is the electron-density contrast-weighted sum of the squares of the atomic distances from the center of mass. The R_g for the energy-minimized conformer of **1** in toluene corresponds to a value of 17.2 Å.

In the region beyond $q = 0.1$ Å^{-1}, the calculated scattering shows a strong oscillatory pattern that reflects the interference produced by X-ray scattering from spatially resolved portions of the molecular array. As to be shown in the following, the characteristic features of this interference pattern, including the oscillatory beat pattern, amplitude, and damping, are sensitively dependent in distinguishable ways upon the macrocycle structure, the configurational dispersion, and interactions with the solvent. The experimental scattering pattern measured for compound **1** in toluene is shown in the lower trace in Figure 2, recorded to 6 Å spatial resolution with 100 seconds of data acquisition under solution flow conditions.

The experimental scattering data generally parallel those calculated for the model and show a transition between small-angle and high-resolution interference scattering near $q = 0.1$ Å^{-1}. While the experimentally measured oscillatory high-angle interference shows significant amplitude dampening compared to the calculated pattern, the interference pattern was highly reproducibly measured with peak positions close to those calculated from the model structure. Detection of the high-angle interference pattern for the porphyrin arrays in toluene is remarkable given that this is a "difficult", low-contrast experiment in which both the solute and solvent have similar atomic compositions. The experiments described herein took advantage of the brilliance of the synchrotron light source to resolve the slight excess high-angle scattering from the dilute ($\leq$1% w/v) macromolecular solute in the presence of significant solution background scattering. Spatial resolution in the experiments presented here was restricted by the geometry of the experimental apparatus, in which the radially symmetric high-angle scattering rings were only partially captured by the corners of the square mosaic detector. Preliminary experiments with shorter sample-to-detector distances show that accurate measurement of high-angle interference patterns for shape-persistent macrocycles in solution can be measured with excellent signal to noise to 2 Å spatial resolution. Further discussion on the experimental data acquisition and reproducibility is provided in the Supporting Information.

Determination of Macromolecular Dimensions and Architectures. Figure 3 shows a comparison of the calculated and experimental scattering patterns for the macrocycle **1** and assembly **1**+**2** measured to a spatial resolution of 7.8 Å. Scattering calculations from the energy-minimized model structures show that insertion of the guest molecule **2** into structure **1** produces several characteristic changes in both the small- and high-angle scattering regions. First, in the small-angle scattering region, a 1.26-fold increase is seen in the total scattering amplitude, $I(0)$, calculated for **1**+**2** relative to **1**. This reflects the increased molecular mass for structure **1**+**2** compared to **1**. Calculated scattering patterns for the energy-minimized array **1** and assembly **1**+**2** yield R_g values of 17.2 and 16.3 Å, respectively. The larger R_g for array **1** despite its smaller mass is primarily due to an increased weighting of electron density in the molecular periphery, with a minor contribution arising from the slight expansion of the porphyrin pair distances a compared to those in the host−guest assembly **1**+**2**. In the high-angle scattering region, the insertion of guest **2** into array **1** is seen to alter the oscillatory interference pattern. Within the experimentally recorded resolution range, these changes include an attenuation of the first interference peak and increased amplitude in the second. A comparison of calculated and experimental scattering patterns in Figure 3 shows that the general features of molecular scattering predicted from structural models for array **1** and assembly **1**+**2** are reproduced in the experimental data. A more detailed comparison follows.

(42) Guinier, A.; Fournet, G. *Small Angle Scattering*; Wiley: New York, 1955.

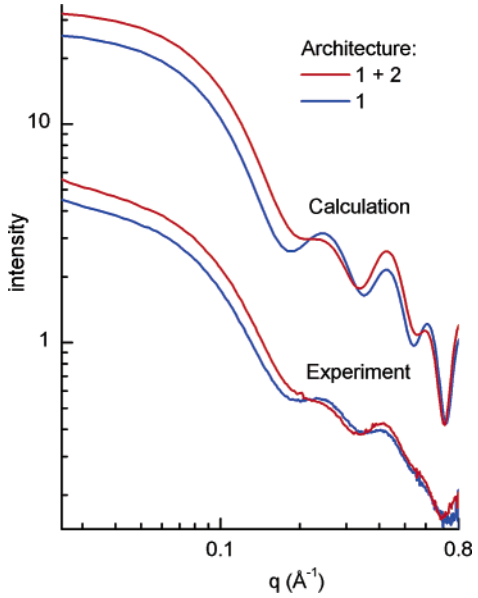

Figure 3. Calculated and experimental X-ray scattering patterns for architectures **1** and **1**+**2**. The upper traces shows the scattering pattern calculated using the coordinates of the energy-minimized conformer **1** (blue) and conformer **1**+**2** (red). The lower traces show experimental scattering patterns measured for 1 mM solutions of compounds **1** and **1**+**2** in toluene. The calculated and experimental pairs of scattering patterns were arbitrarily offset.

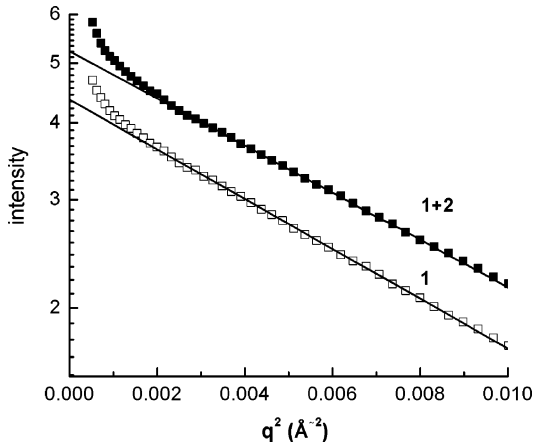

Figure 4. Guinier plots for experimental small-angle scattering data for macrocycle **1** and assembly **1**+**2**. The solid lines are fits to the experimental data using the Guinier approximation, with R_g values of 16.7 (±0.1) Å and 16.3 (±0.1) Å and I(O) values of 5.23 (±0.01) and 4.36 (±0.01) for **1** and **1**+**2**, respectively. The experimental error bars are equal to or smaller than the plotted symbols.

Guinier analysis in the small-angle scattering region provides a measure of the forward scattering amplitudes, I(0), and radii of gyration of the molecular assemblies, R_g.[13,42] Fits to experimental scattering in the small-angle Guinier region 0.04 Å^{-1} < q < 0.1 Å^{-1} yield I(0) values of 4.36 (±0.01) and 5.23 (±0.01) and R_g values of 16.7 (±0.1) Å and 16.3 (±0.1) Å for array **1** and assembly **1**+**2**, respectively (Figure 4). The 1.20-fold increase in I(0) measured for **1**+**2** compared to **1** is comparable to the predicted mass increase of 1.26 and provides experimental demonstration of the formation of a stoichiometric 1:1 complex of the host **1** with the tripyridyl guest **2**. The smaller R_g measured for assembly **1**+**2** compared to array **1** is also predicted from the model structures, and the experimental value is in good agreement with the value calculated from the energy-minimized **1**+**2** model structure. However, the experimentally determined R_g for array **1** is 0.5 Å smaller than that calculated from the model. The small-angle scattering measurements indicate that although the molecular mass for array **1** is consistent with the model, its solution structure deviates from the model by having a smaller R_g. The nature of the structural variation cannot be resolved from measurements in the small-angle scattering region.

In the **q**-range below 0.04 Å^{-1} (below q^2 = 0.002 Å^{-2} in the Guinier plots, Figure 4), experimental scattering data for both architectures show concentration-dependent upward deviations from the predicted Guinier scattering behavior that are characteristic of weakly associating ("sticky") molecular systems.[13,43] For example, we have observed this type of behavior for other molecular[44] and micellar[45] systems having neutral or near-neutral net charge, and we have observed the opposite, electrostatically driven repulsive deviations in strongly charged molecular,[21] micellar,[46] and colloidal[47] systems. In the present case, the deviations from expected Guinier relationships at low q suggest that toluene is not an optimal solvent for the porphyrin arrays by leaving sites for weak, likely geometrically nonspecific, molecular self-association. Preliminary experiments indicate that carbon disulfide and binary mixtures of carbon disulfide with toluene may serve as better solvents, as scattering patterns measured for array **1** did not deviate from ideally monodispersed scattering behavior at low q. Comparison of the details of the high-angle scattering patterns as a function of solvent provides the interesting possibility of investigating the structure of the macrocycle−solvent interface. However, experiments of this type are complicated by the large change in electron-density contrast between the macrocycle and solvent and the high X-ray absorption cross sections of the non-hydrocarbon solvents. Examination of solvent-dependent characteristics of the porphyrin macrocycle scattering will be addressed in a separate report.

The sensitivity of high-angle interference patterns to the dimensions of the molecular configuration is demonstrated by a comparison of calculated scattering patterns for three conformers that show progressive shifts in the dimensions for array **1** as illustrated in Figure 5. Trace 1 is the scattering pattern calculated from the minimized conformer **1** discussed above and trace 2 was calculated from the minimization starting structure, denoted conformer **1**$^{\mathbf{a}}$. Trace 3 was calculated from a higher energy conformer, denoted **1**$^{\mathbf{b}}$, with distortions in the diphenylethyne linkers that shortened the diphenylethyne linkers by 0.7 Å. Compared to the energy-minimized conformer, conformers **1**$^{\mathbf{a}}$ and **1**$^{\mathbf{b}}$ expand and contract the array diameter by 2.2 and 1.2 Å, respectively. In each of these conformers, the perpendicular orientations of the porphyrin planes and the approximate threefold symmetry of the array were preserved. The conformers were chosen to differ mainly in the dimensions of the array. Figure 6 shows an overlap of the structures for conformers **1** and **1**$^{\mathbf{b}}$. The calculated scattering patterns reflect the structural analogies by showing the characteristic interference beat pattern to be conserved, but with the changes in dimension

(43) Ducruix, A.; Guilloteau, J. P.; Ries-Kautt, M.; Tardieu, A. *J. Cryst. Growth* **1996**, *168*, 28−39.
(44) Marone, P. A.; Thiyagarajan, P.; Wagner, A. M.; Tiede, D. M. *J. Cryst. Growth* **1998**, *191*, 811−819.
(45) Thiyagarajan, P.; Tiede, D. M. *J. Phys. Chem.* **1994**, *98*, 10343−10351.
(46) Chen, S. H.; Sheu, E. Y.; Kalus, J.; Hoffman, H. *J. Appl. Crystallogr.* **1988**, *21*, 751−769.
(47) Rajh, T.; Thurnauer, M. C.; Thiyagarajan, P.; Tiede, D. M. *J. Phys. Chem.* **1999**, *103*, 2172−2177.

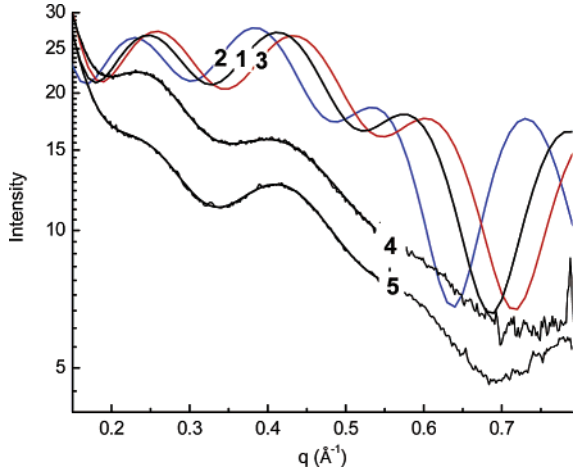

Figure 5. Scattering as a function of supramolecular dimension. Traces 1−3 show calculated scattering for three conformations of the array **1**, corresponding to (1) the energy-minimized conformer **1**, (2) the starting structure used in the minimization, **1**^{a}, and (3) a conformer with distortions in the diphenylethyne linkers, **1**^{b}, with corresponding supramolecular radii of 16.9, 18.0, and 16.3 Å. Traces 4 and 5 show experimental data along with superimposed Gaussian fits to the first two peaks for compounds **1** and **1**+**2**, respectively.

Figure 6. Comparison of the structures for the energy-minimized conformer **1** (black) and the higher energy conformer **1b** (red).

reflected by shifts in the positions of the scattering patterns in the q-domain. The calculated scattering patterns show that even the relatively subtle 1.2 Å changes in the dimensions of conformers **1** and **1**^{b} produce shifts in the interference peak positions that are large, $\Delta q > 0.01$ Å^{-1}, compared to the experimental resolution of peak positions, identified in the lower portion of Figure 5 by fitting experimental scattering patterns with Gaussian line shapes to a standard deviation of 0.001 Å^{-1}. This precision in the determination of peak positions in experimental scattering data in q-range above 0.4 Å^{-1} translates to a precision of 0.1 Å in the determination of molecular dimensions. Scattering patterns calculated for conformers with large deviations from the approximate threefold symmetry of structure **1** show characteristic changes in the oscillatory beat pattern and peak positions, demonstrating that the high-angle scattering data contains precise information on the shape and dimensions of the molecular architectures.

Direct comparisons between the reciprocal-space scattering patterns and real-space molecular models can be made through

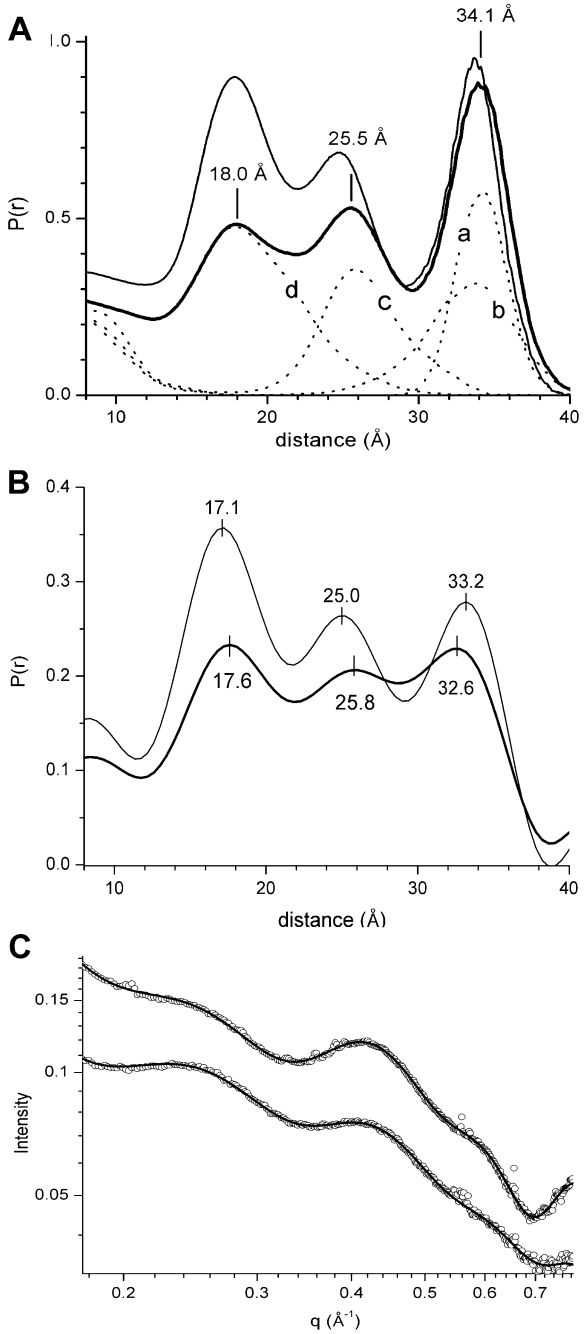

Figure 7. Atomic pair distance distribution function, PDF, analysis. Part A shows the PDF calculated from the energy-minimized structures **1** (thick line) and **1**+**2** (thin line). The dashed lines show the PDF for the porphyrin pairs that comprise array **1**, labeled according to the scheme depicted in Figure 1. Part B shows experimentally determined PDF obtained by fitting to experimental scattering data for compounds **1** and **1**+**2** using GNOM.[24,25] Part C shows the fit of the Fourier transformed PDF to experimental data.

comparison of the atomic pair distance distribution functions, PDF. Figure 7A shows PDF patterns calculated from the atomic coordinates for energy-minimized conformers **1** (thick line) and **1**+**2** (thin line). The PDFs resolved into characteristic three-peak patterns within the region of spatial resolution for the experimental scattering data. The dashed lines plotted underneath these curves show the PDF calculated for the four sets of porphyrin pairs that comprise array **1**, with labels corresponding to the porphyrin pairs indicated in Figure 1. Each of the peaks

in the PDF is seen to be associated with specific porphyrin pairs. The first peak at 34.1 Å arises from atom pair correlations between Fb−porphyrin/Zn−porphyrin pairs **a**, and the corner, Zn−porphyrin/Zn−porphyrin pairs **b**. The porphyrin pair PDF peak positions are sensitive to both the center-of-mass distance separations of the porphyrins and their relative angles. For example, the parallel orientations of pairs **a** create a more symmetric, narrow distribution compared to the canted orientations of pairs **b**. This long-range peak defines an effective diameter of the assembly. The next-to-nearest-neighbor Zn−porphyrin/Zn−porphyrin pairs **c**, and the nearest-neighbor Zn−porphyrin/Fb−porphyrin pairs **d** make dominant contributions to the PDF peaks at 25.5 and 18.0 Å, respectively. The well-resolved three-peak PDF pattern was a characteristic feature of the symmetric, cyclic supramolecular architecture.

In the model studies, insertion of the tripyridyl guest **2** into array **1** followed by reminimization of the assembly **1**+**2** produced a slight doming of the Zn−porphyrin rings without appreciable shifts in other atomic positions. This atomic rearrangement produced a shift in the PDF peak for pairs **a**+**b** to 33.7 Å and a shift of the peak **c** to 24.8 Å. Comparisons of PDF patterns for architectures **1** and **1**+**2** show that the presence of the guest molecule within the host assembly produces new atom pair correlations that fall throughout the distance range below 30 Å. These new correlations between the guest and host contribute to the "background" in the PDF pattern surrounding the porphyrin pair peaks **c** and **d** for the assembly **1**+**2**. Atomic pair correlations with guest **2** do not contribute appreciably to the porphyrin pair peak **a**+**b** for the assembly **1**+**2**.

Experimentally determined PDFs for **1** and **1**+**2** in toluene are shown in Figure 7B, obtained using the X-ray scattering fitting program GNOM.[25,48] Fourier transforms of the fitted PDFs to scattering patterns and comparisons of the ensuing fits to data are shown in Figure 7C. The resulting experimentally determined PDFs exhibit three-peak patterns that are analogous to those obtained from model structures. Resolution of this three-peak PDF pattern provides the following key parameters on the porphyrin solution-state structures: (1) Determination of the overall dimensions of the macrocyclic architectures by resolution of the individual porphyrin pair distance correlations; (2) identification of the cyclic, approximately threefold symmetric shape of the array by comparison of experimental and calculated PDF patterns; and (3) characterization of the conformational dispersion of the macrocyclic arrays measured through a broadening of the atomic pair distance correlations; however, model calculations show that the experimentally determined PDF line widths are partially broadened by limited spatial resolution of the current scattering measurements, and as discussed below, an estimate of conformational dispersion can be better assessed by examination of the dampening of high-angle scattering patterns. Overall, the high-angle scattering measurements provided a direct verification of the cyclic hexameric shape and general correspondence between experimental and targeted model structures.

The experimentally determined position of the PDF peak **a**+**b** for compound **1** is 32.6 Å, and corresponds to a 1.5 Å decrease from the peak position calculated from model **1**. The experimental **c** and **d** peaks are 0.3 and 0.4 Å shorter than those calculated from the model structure. The experimentally determined PDF for assembly **1**+**2** shows that insertion of the tripyridyl guest **2** into **1** causes an expansion of the effective diameter of the assembly by about 0.6 Å, bringing the resulting 33.2 Å array diameter closer to the 33.8 Å diameter predicted from the model **1**+**2** structure.

Evaluating Amplitudes of Rigid-Body Porphyrin Motions. As outlined in the Supporting Information, we have developed analytical methods for evaluating effects of atomic thermal factors and harmonic rigid-body motions on experimental X-ray scattering measurements.[20,21,49] These methods were applied to the hexameric porphyrin architecture by breaking the macrocycle into atomic groups that included each porphyrin and the attached phenyl and mesityl rings. Configurational dispersions created by harmonic rigid-body group motions were characterized by atomic displacement vectors, $\mathbf{u}_i$. This result is analogous to the use of Debye−Waller approximation for describing the effect of atomic thermal factors on diffraction[50] but is used here as a parameter describing motion for a group of atoms.

Several types of random rigid-body motions were considered, including independent rotation and translation of individual porphyrin groups within the cyclic architecture and concerted motions of two or more groups moving as intact fragments. These studies provide a method to outline the conformational envelope of a supramolecular assembly. For example, Figure 8A shows scattering calculated for model conformer **1** as a function of the dispersion in the radial position of the porphyrin groups. Harmonic disorders of 2 and 3 Å amplitudes are seen to progressively dampen oscillatory scattering features in a q-dependent manner.

A comparison of experimental scattering data for array **1** with 3 Å positional disorder is shown in Figure 8B, along with a calculated scattering for a model based on conformer **1** that includes a full 360° porphyrin group rotational disorder around the diphenylethyne linker axes. For the model calculations in Figure 8B, the scattering q-range was scaled to allow alignment of experimental and calculated scattering peaks. This adjustment accounts for the 5% reduction in the dimensions of the experimental array compared to conformer **1**. Compared to the data, 3 Å positional disorder can be seen to produce a slight overdampening of the oscillatory pattern that is noticeable with the higher-angle peak at $q = 0.4$ Å^{-1} and trough at $q = 0.7$ Å^{-1}. Conversely, complete rotational disorder is seen to produce an overdampening of the first interference peak at $q = 0.25$ Å^{-1} but an underdampening of the higher-angle scattering peaks. These calculations set limits for the rigid-body motions that are consistent with experimental dampening patterns. The data point to a solution-state ensemble with mean molecular dimensions 5% shorter than those of conformer **1**, and with a conformational envelope that has as limits 3 Å positional dispersion or 360° rotational freedom for all six porphyrin groups, or lower amplitude combinations of both of these motions. Interestingly, the high-angle interference trough at $q = 0.7$ Å^{-1} is experimentally much better resolved for the assembly **1**+**2** compared to array **1**. The analytical models suggest that this result corresponds to configurational dispersion for assembly **1**+**2** that is reduced by about a factor of 2 compared to **1**.

(48) Svergun, D. I.; Semenyuk, A. V.; Feigin, L. A. *Acta Crystallogr.. Sect. A* **1988**, *44*, 244−250.
(49) Zhang, R.; Marone, P. A.; Thiyagarajan, P.; Tiede, D. M. *Langmuir* **1999**, *22*, 7510−7519.
(50) Warren, B. E. *X-ray Diffraction*; Dover Publications: New York, 1990.

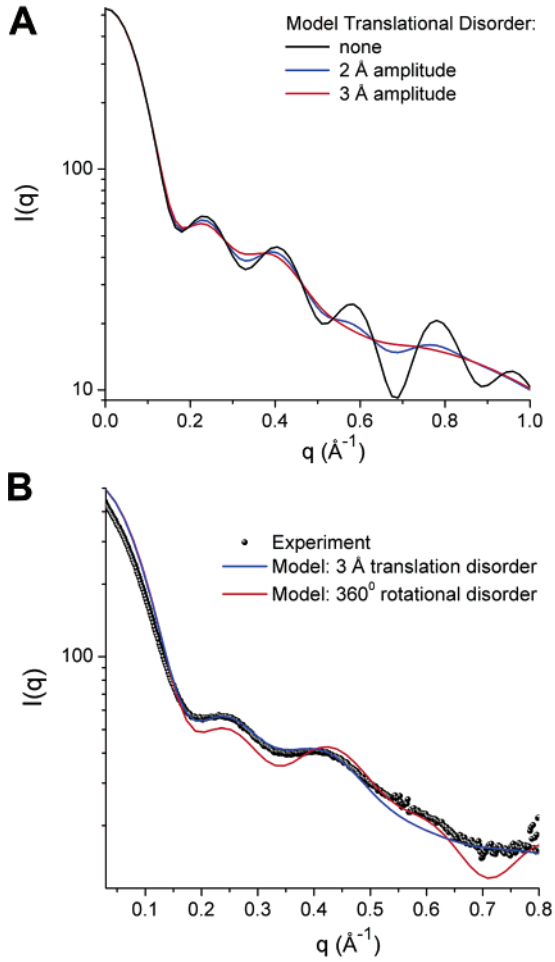

Figure 8. Effect of rigid-body porphyrin motions on high-angle scattering for array **1**. Part A shows scattering patterns calculated using conformer **1** as an equilibrium structure and having porphyrin group harmonic translational disorders of 0 Å (black), 2 Å (blue), and 3 Å (red) amplitudes. Part B shows a comparison of experimental scattering data for array **1** with a model structure experiencing 3 Å translational disorder (blue line) and alternatively a full 360° rotational disorder (red line). Both the model calculations in part B used the model structure **1**, but the calculated scattering **q**-range was scaled to allow alignment of experimental and calculated scattering peaks. This adjustment accounts for the 5% reduction in the dimensions of the experimental array compared to model structure **1**.

Correlations are found between analytical and molecular models for disorder. For example, Figure 9 shows sets of three snapshots taken from the final 100 ps of 1 ns molecular dynamics simulations for array **1** and assembly **1**+**2**. The conformations reflect fluctuations within thermally equilibrated molecular systems. For array **1**, the individual conformers display a range of distortions that notably include bowing distortions and rotation of all six porphyrin groups. These distortions are approximated by the rigid-body position and rotational dispersions described above. Several of the conformers show porphyrin pair **a**+**b** PDF peaks to be shorter than the 34.1 Å distance calculated from the energy-minimized, planar conformer **1**. One example is the central conformer depicted in Figure 9A. The experimental PDF patterns demonstrate that the solution ensemble average is centered on conformers of this type that reduce the overall molecular dimensions. The right and left conformers in Figure 9A illustrate distortions from the equilibrium structure that combine rotational and porphyrin group bowing distortions required to account for dampening of the high-angle scattering patterns. Figure 9B shows snapshots

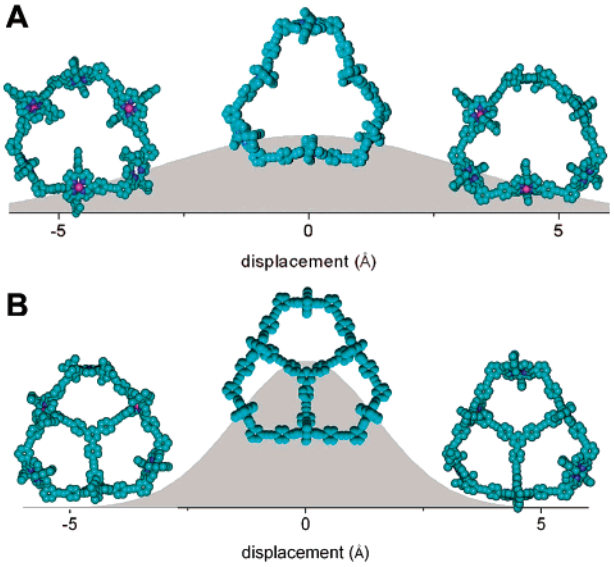

Figure 9. Snapshots of conformers observed within molecular dynamics simulations for array **1** (Part A) and assembly **1**+**2** (Part B). The snapshots are plotted on top of configuration dispersions estimated from broadening of experimental scattering patterns using a rigid-body porphyrin positional dispersion model. The conformers for array **1** show extensive bowing distortions and rotations of all six porphyrin groups. Assembly **1**+**2** shows an expanded equilibrium conformation with a restricted set of distortions.

taken from a molecular dynamics simulation of **1**+**2**. Scattering data demonstrate that the dimensions of the equilibrium structure for **1**+**2** are expanded by 0.6 Å compared to **1** and that this shift can be accounted by the removal of porphyrin bowing distortions by the tripyridyl guest. The preliminary molecular dynamics simulations also show a more restricted set of distortions compared to **1**, consistent with the experimentally estimated 2-fold reduction in the amplitude of the structural dispersion in solution. A detailed comparison of high-angle molecular scattering data with conformational ensembles generated by molecular dynamics simulations will be presented in a subsequent publication.

Conclusions

High-angle X-ray scattering measurements are demonstrated to provide a new method for direct structural verification and analysis of shape-persistent macrocycles in solution. Structural features resolved for array **1** and host−guest assembly **1**+**2** in aromatic hydrocarbon solvents included the following: (1) demonstration of the cyclic hexameric structure of the porphyrin array through resolution of the characteristic three-peak porphyrin pair distance correlations; (2) measurement of the amplitude of the configurational dispersion for array **1** in solution and resolution of a 1.5 Å shortening of the ensemble-averaged dimensions for array **1** compared to an energy-minimized planar porphyrin model structure; and (3) measurement of a 0.6 Å expansion of the cyclic hexameric porphyrin host assembly upon guest insertion and approximate 2-fold decrease in the amplitude of the configurational dispersion. These structural features are summarized in Figure 9. Resolution of long-range, nanoscale structural features of shape-persistent macrocycles has previously proven to be difficult in the absence of crystal structures.[1−3,11] Even though crystal structures can eventually hoped to be obtained for each of the molecular assemblies of interest, high-resolution scattering measurements

of the type outlined here provide unique information on the characteristic conformational landscapes for the supramolecular architectures in liquids that cannot be accessed by crystallographic studies.

Proof of the cyclic hexameric structure of macrocycle **1** has previously rested on precise measurements of molecular mass and composition.[4] While these measurements provide definitive evidence of the cyclic architecture and Zn_3Fb_3 hexameric composition of the assembly, they cannot provide information on structural characteristics. The damped oscillatory high-angle scattering patterns measured for macrocycle **1** combined with PDF analyses provided a direct measure of the molecular dimensions and shape through resolution of the three sets of porphyrin pair distance correlations. The data demonstrate that macrocycle **1** cannot be characterized by a single conformation but exists in an ensemble skewed toward conformers having an average 1.5 Å shortening of the porphyrin pair **a**+**b** distances compared to an energy-minimized planar porphyrin model structure. The shortened porphyrin pair correlation distances indicate that the average conformation for macrocycle **1** in solution has bowed distortions of the porphyrin and diphenylethyne linker groups. Conformers of this type are apparent in energy minimization studies and molecular dynamics simulations. Analytical models estimate the limits of the conformational envelope to include 3 Å dispersion in porphyrin group positions and full rotational freedom. However, combinations of multiple motions of lower amplitude will likely provide the best fit to experimental scattering.

Insertion of the guest molecule **2** into macrocycle **1** expanded the dimensions of the macrocycle by 0.6 Å and restricted the configurational dispersion by about a factor of 2. The structural changes bring the model and experiment into closer agreement. These results suggest a role for the guest molecule in restricting the range of conformers accessed by the assembly.

Control of the conformational landscape is potentially critical for achieving control of solution-state chemistry. For example, doming and nonplanar distortions play a significant role in determining porphyrin excited-state decay processes and lifetimes.[51,52] Further, the energy and electron/hole transfer processes in these diphenylethyne-linked multiporphyrin architectures occur predominately via through-bond mechanisms.[33] Porphyrin geometric distortions and through-bond couplings are likely to be modulated by bond torsions, bending, and rotational distortions that are manifest in the solution-state configurational disorder. This work suggests the opportunity of making concomitant measurements of photochemistry and configurational disorder as a function of temperature, solution-state parameters, and molecular design for resolving the effects of architectural dynamics on energy- and electron-transfer efficiencies.

Finally, while small-angle X-ray scattering has long been recognized as a tool for low-resolution structural characterization of macromolecules in solution,[13,42] the experiments presented here demonstrate the new opportunity of using high-angle X-ray scattering for higher resolution studies. Indeed, we anticipate that shorter sample-to-detector distances will enable accurate measurements with excellent signal to noise to 2 Å spatial resolution. The relatively short acquisition times (1−2 min), dilute solutions (1 mM), and small liquid sample volumes ($\leq$50 μL) make these measurements amenable for automated, high-throughput applications. In this regard, high-angle X-ray scattering should provide a valuable and perhaps unique tool for gaining a deeper understanding of the structure and conformational landscape of diverse supramolecular architectures in solution.

Acknowledgment. This work was supported by the Office of Basic Energy Sciences, Divisions of Chemical (D.M.T., R.Z., and L.X.C.) and Material Sciences (Advanced Photon Source), U.S. Department of Energy, under contract W-31-109-ENG-38, and grant DE-FG02-99ER14632 (L.Y. and J.S.L.). Special appreciation is acknowledged to the APS-BESSRC staff, especially Drs. Soenke Seifert, Jennifer Linton, Guy Jennings, Mark Engbretson, and Mark Beno, whose talents and tireless efforts made these synchrotron experiments possible, and to Drs. Xiaobing Zuo and Andrew Goshe for numerous insightful discussions on molecular scattering.

Supporting Information Available: Experimental Methods; X-ray scattering measurements; figure showing raw experimental scattering patterns for the macrocycle **1** solution (1 mM in toluene) and the solvent (toluene) separately; coordinate-based X-ray scattering analysis and effects of rigid-body motions with 11 equations; molecular modeling calculations. This material is available free of charge via the Internet at http://pubs.acs.org.

JA048209Q

(51) Sazanovich, I. V.; Galievsky, V. A.; van Hoek, A.; Schaafsma, T. J.; Mallnovskii, V. L.; Holten, D.; Chirvony, V. S. *J. Phys. Chem. B* **2001**, *105*, 7818−7829.
(52) Ogura, H.; Yatsunyk, L.; Medforth, C. J.; Smith, K. M.; Barkigia, K. M.; Renner, M. W.; Melamed, D.; Walker, F. A. *J. Am. Chem. Soc.* **2001**, *123*, 6564−6578.